Heliyon

Received:
22 November 2018
Revised:
11 March 2019
Accepted:
4 April 2019

Cite as: Takaaki Tanaka, Yoshihiko Takai, Akifumi Nagase, Kazuki Teraguchi, Hiromi Minbu, Akihito Ochiai, Isao Kimura, Masayuki Taniguchi. Protein adsorption characteristics of nanoparticle-assembled hollow microspheres of hydroxyapatite and their composites with PLLA microporous membranes. Heliyon 5 (2019) e01490.
doi: 10.1016/j.heliyon.2019.e01490

Protein adsorption characteristics of nanoparticle-assembled hollow microspheres of hydroxyapatite and their composites with PLLA microporous membranes

Takaaki Tanaka [a,*], **Yoshihiko Takai** [a], **Akifumi Nagase** [a], **Kazuki Teraguchi** [a], **Hiromi Minbu** [a], **Akihito Ochiai** [a], **Isao Kimura** [b], **Masayuki Taniguchi** [a]

[a] *Department of Materials Science and Technology, Niigata University, Niigata 950-2181, Japan*

[b] *Department of Chemistry and Chemical Engineering, Niigata University, Niigata 950-2181, Japan*

[*] Corresponding author.

E-mail address: tctanaka@eng.niigata-u.ac.jp (T. Tanaka).

Abstract

Nanoparticle-assembled hydroxyapatite (HA) hollow microspheres have a high surface area and are convenient to handle, owing to their characteristic structure. In this study we characterized the protein adsorption of HA hollow microspheres prepared from $CaCl_2$ and K_2HPO_4 by a water-in-oil-in-water (W/O/W) emulsion method assisted by two surfactants: Span 80 and Tween 20. The HA hollow microspheres adsorbed bovine serum albumin, bovine γ-globulin, equine skeletal muscle myoglobin, and chicken egg white lysozyme in 10 mM sodium phosphate buffer (pH 6.8) in a Langmuir-type adsorption and desorbed the proteins in 800 mM sodium phosphate buffer (pH 6.8). The maximum adsorbed amounts of the HA hollow microspheres were 7.5−9.0 times higher than those of the microrods with a similar size range. The composite membranes of the HA microspheres and the poly(L-lactic acid) (PLLA) microporous membranes exhibited a high adsorption capacity for γ-globulin.

https://doi.org/10.1016/j.heliyon.2019.e01490

Keywords: Materials science, Materials chemistry, Physical chemistry

1. Introduction

Hydroxyapatite (HA) is the major inorganic solid component in bones, and has high affinity with various proteins including collagen, which composes the bones using this inorganic component [1]. HA has phosphate cites whose negative charge interacts with amino groups of proteins and calcium cites whose positive charge does with carboxyl groups of them. Thus, various proteins are adsorbed on HA and HA has been used as one of the major adsorbents in protein chromatography [2]. Many types of HA materials are prepared for bone repair materials and adsorbents [3, 4]. HA particles, some of which are sintered to form HA blocks, can be synthesized from calcium and phosphate ions. Various types of HA particles, with different size and shape, have been synthesized under various conditions [5, 6]. Amongst them, nanoparticle-assembled hollow microspheres provide advantages to adsorbents because they have higher specific areas for adsorption in comparison with simple microspheres and are more convenient to handle in comparison with nanoparticles [5, 7, 8]. Hollow HA microspheres can be synthesized using various methods including spray drying [9], solvothermal/hydrothermal synthesis [6, 10, 11], conversion $CaCO_3$ microspheres [12, 13, 14] and Li_2O-CaO-B_2O_3 [15,16], and assembly approaches with organic/inorganic materials. In assembly approaches, surfactants [17, 18], amino acids [19], polymers [20, 21, 22], and yeast cells [23] have been used to form hollow microspherical structures.

In this study, we applied nanoparticle-assembled hollow HA microspheres prepared by a water-in-oil-in-water (W/O/W) emulsion method [17] to the adsorption of various proteins. The W/O/W emulsion method is a facile technique that can be executed using very common apparatus. Because the morphology of the product is based on the inner aqueous phase droplets, it can be controlled at the primary emulsification stage with various surfactants [24]. Two different kinds of surfactants are used for the formation of W/O/W emulsion. Lipophilic surfactants, e.g. Span 80 (hydrophilic-lipophilic balance (HLB) value: 4.3) [25,26], and hydrophilic surfactants, e.g. Tween 20 (HLB value: 16.7) [25,27], stabilize W/O and O/W emulsions, respectively. Calcium ions in the outer aqueous phase diffuse through the oil phase to the interface between the oil phase and the inner aqueous phase, where they react to produce HA nanocrystals and consequently to form microspheres (Fig. 1 (a)) [17]. The adsorption characteristics of the hollow HA microspheres by the W/O/W emulsion method were compared with those of commercially available microrod-type HA crystals. Additionally, the microspheres were integrated into a microporous membrane and the composite membrane was used to recover the proteins.

https://doi.org/10.1016/j.heliyon.2019.e01490

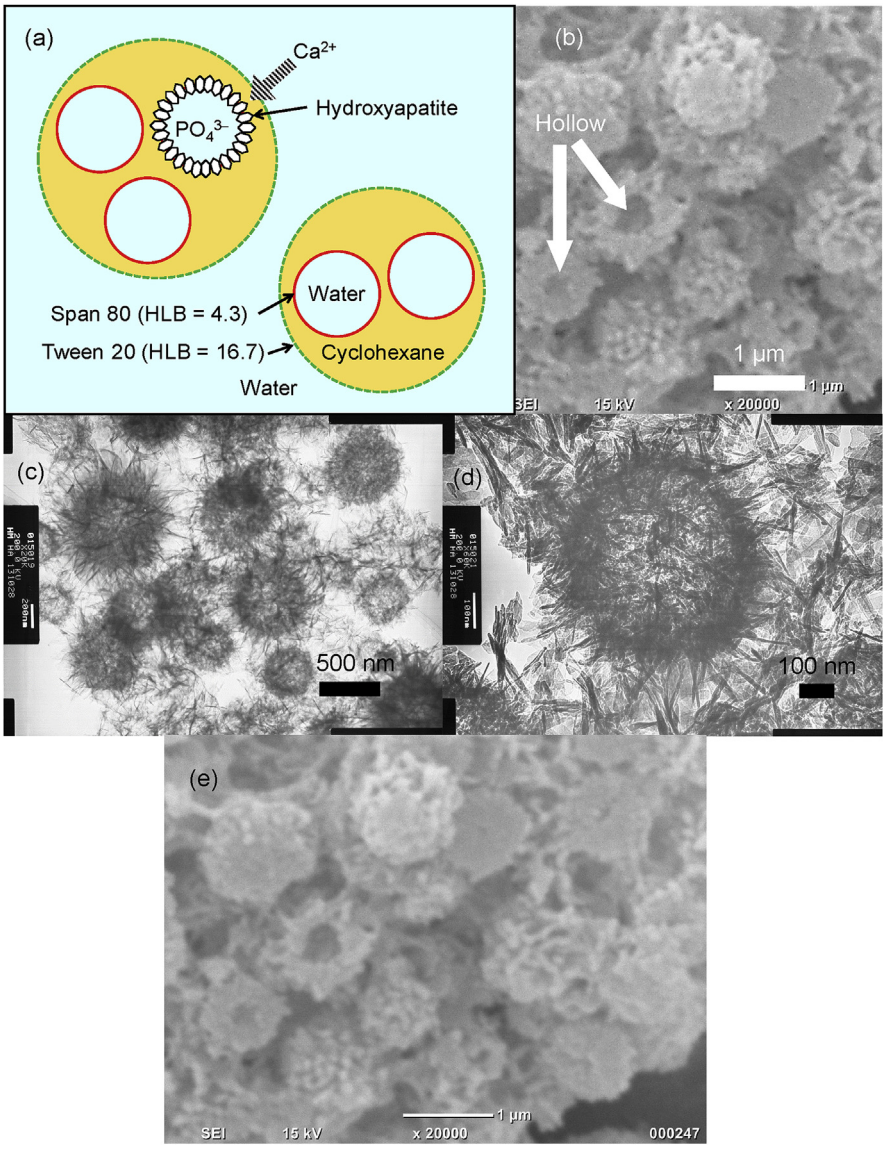

Fig. 1. Interfacial synthesis (a) and SEM (b) and TEM (c, d) images of HA hollow microspheres. Fig. 1(e) is the original figure of Fig. 1(b) before cropping and tuning of the sharpness (+70%).

2. Materials and methods

2.1. Materials

Cyclohexane, $CaCl_2$, K_2HPO_4, and KOH were purchased from Wako Pure Chemical Industries and were of analytical grade. The three types of surfactants, namely, Span 80 (sorbitan monooleate), Tween 20 (polyoxyethylene (20) sorbitan monolaurate), and Tween 80 (polyoxyethylene (20) sorbitan monooleate) (a hydrophilic surfactant, HLB value: 15) [25], were reagent grade products of Wako Pure Chemical Industries. Commercially available HA (Apatite HAP, monoclinic, Wako Pure

https://doi.org/10.1016/j.heliyon.2019.e01490

Chemical Industries) was used as the HA microrods, for comparison. KBr for infrared (IR) analysis was purchased from Wako Pure Chemical Industries. Four proteins, namely, bovine serum albumin (A3059), bovine γ-globulin (G5009), equine skeletal muscle myoglobin (M0630), and chicken egg white lysozyme (L6876), were obtained from Sigma-Aldrich. Poly(L-lactic acid) (PLLA) was a gift from Toyota Motor Corp. The PLLA properties included the weight average molecular weight: 1.22×10^5 ($M_w/M_n = 3.0$), optical purity: 98.5%, melting point: 174.0 °C, and glass transition temperature: 59.7 °C. Analytical grade 1,4-dioxane was purchased from Wako Pure Chemical Industries. All chemicals were used without further purification.

2.2. Preparation of HA hollow microspheres

The HA hollow microspheres were synthesized by a modified interfacial reaction in a W/O/W emulsion [17]. The inner aqueous phase was prepared by adjusting the pH of a 0.30 M K_2HPO_4 solution to 12 with KOH flakes. Cyclohexane was used as the oil phase where Span 80 was dissolved at 5.0% as a stabilizer for the interface between the inner aqueous and oil phases. The outer aqueous phase included 0.50 M of $CaCl_2$ and 0.50% of Tween 20 as the stabilizer for the interface between the oil and outer aqueous phases. To prepare a W/O emulsion, 40.5 mL of the inner aqueous phase and 94.5 mL of the oil phase were mixed and agitated for 5 min at 12,000 rpm using a homogenizer. Then, the emulsion was poured into 315 mL of the outer aqueous phase in a 500-mL separable flask equipped with a 40-mm six-bladed disk turbine-type impeller and four baffles. The HA synthesis in the W/O/W emulsion was conducted at 50 °C and 300 rpm for 24 h. The reaction product was washed with cyclohexane, acetone, and water in sequence, collected with centrifugation, and then freeze-dried to remove the water.

2.3. Preparation of PLLA membranes

Asymmetric PLLA membranes were prepared using a previously reported nonsolvent-induced phase separation method [28]. In this study, a solution of 3.75 g PLLA, 6.95 g of Tween 80, and 45.25 g of 1,4-dixoxane was cast on a 0.5 mm-deep mold of glass and polytetrafluoroethylene. Then, the solution in the mold was immersed into a water bath. The formed membrane was extensively washed with water.

2.4. Preparation of HA-PLLA composite membranes

HA-PLLA composite membranes were prepared by filtering the suspensions of the HA hollow microspheres with asymmetric PLLA membranes from their rough sides. A 25-mm circular PLLA membrane was set on a dead-end filtration cell (amicon

https://doi.org/10.1016/j.heliyon.2019.e01490

8010, 4.1 cm^2, Merck Millipore) without its stirring assembly. A suspension of 20 mg HA microspheres in 50 mL of 10 mM sodium phosphate buffer (pH 6.8) was filtered at a speed of 3 mL/h with a peristaltic pump (SMP-1, EYELA). The composite membrane formed after approximately 20 h of filtration.

2.5. Characterization of HA hollow microspheres

The crystalline phase of the HA hollow microspheres was identified by X-ray powder diffraction (XRD) with the CuKα irradiation of an X-ray diffractometer (RINT 2500HR/PC, Rigaku). Fourier transform IR (FTIR) absorption spectroscopy was performed using the KBr method (IRAffinity-1S, Shimadzu). The specific surface area of the microspheres was measured with a surface area and porosity analyzer (Tristar II 3020, Micromeritics). The morphology of the microspheres was observed mainly by scanning electron microscopy (SEM; JCM-6000, JEOL, and TM-1000, Hitachi) after sputter coating with Au-Pd (MSP-1S, Vacuum Device). The wet filtration cakes of the HA microspheres in the PLLA membrane fractured after being frozen in liquid nitrogen to observe the internal structure of the microspheres. When measuring the size of the microspheres a drop of suspension in methanol was placed on a glass coverslip, and the dispersion medium was evaporated at room temperature. Then, the microspheres and coverslip were coated with Au-Pd. Transmittance electron microscopy (TEM) images of the microspheres on a micro grid (STEM 150 Cu Grid with carbon film, Okenshoji) were taken at 200 kV with JEM-2010 (JEOL).

2.6. Observation of HA-PLLA composite membranes

A wet HA-PLLA composite membrane was fractured after freezing in liquid nitrogen. The membrane was coated with carbon using a carbon coater (CC-50, Shimadzu). The cross-section of the membrane was observed by scanning electron microscopy with energy dispersive X-ray spectroscopy (EDS; JCM-6000 with JED-2300, JEOL).

2.7. Protein adsorption/desorption experiments

In the batch adsorption experiments, the protein solutions were prepared in the range of 100−5000 μg/mL in 10 mM sodium phosphate buffer (pH 6.8). Twenty milligrams of HA hollow microspheres or HA microrods were suspended in the protein solutions at 0−4 °C. The volume of the protein solutions (1−40 mL) was varied such that the adsorption ratio became 5−95% after preliminary experiments with solutions of 1 mL. The protein was adsorbed in the HA microspheres for 2 h by shaking the suspension every 30 min. The supernatant was recovered after centrifugation was applied for 5 min. The protein concentration was measured using the bicinchoninic

https://doi.org/10.1016/j.heliyon.2019.e01490

acid method (BCA Protein Assay Kit, Thermo Scientific) with the used protein in the same buffer to produce a calibration curve. If necessary, the supernatant was diluted with the same buffer.

In the desorption experiments, 800 mM sodium phosphate buffer (pH 6.8) was used as the eluent. The protein-adsorbed HA hollow microspheres or HA microrods were suspended in the buffer at 0−4 °C. Protein desorption was performed for 2 h by shaking the suspension every 30 min. The supernatant was recovered after centrifugation was performed for 5 min, and the protein concentration was measured using the BCA method as described above.

In the protein adsorption experiments with an HA-PLLA composite membrane, 10 mL of 50 μg/mL protein solution in 10 mM sodium phosphate buffer (pH 6.8) was circulated through the membrane on a filtration cell with a peristaltic pump for 2 h at room temperature. The solution was recovered; then, the membrane was washed with 1 mL of 10 mM sodium phosphate buffer (pH 6.8). The elution was performed by circulating 1 mL of 800 mM sodium phosphate through the membrane for 2 h (1st desorption). Then, another 1 mL of the same buffer was circulated for 2 h (2nd desorption). The protein concentrations were measured using the BCA method as described above.

3. Results and discussion

3.1. Synthesis and characterization of HA hollow microspheres

In this study, the HA hollow microspheres were synthesized with $CaCl_2$ and K_2HPO_4, whereas they were synthesized with $Ca(NO_3)_2$ and K_2HPO_4 in a previous study [17]. The advantage of our present approach is the elimination of risk with regard to NO_3^- contamination in the product. Approximately 20 × 200 nm rod-shaped nanoparticles were synthesized radially on the interface between the inner aqueous and oil phases to form the shell structure (Fig. 1(a)). The shell structure was confirmed by SEM and TEM images. The SEM image (Fig. 1(b)) shows the hollows of the microspheres, which were trapped in a membrane after filtration of their suspension followed by cracking in liquid nitrogen. The cracked hollow microspheres could not be observed by TEM. However, the TEM images in Figs. 1(c) and (d) show the shells of the microspheres in their round edges. Note that the microspheres larger than 1 μm were difficult to observed at the magnification of 20000 and 60000 by TEM. The syntheses of inorganic hollow microspheres and microcapsules by W/O/W interfacial reaction have been reported in similar conditions. In addition to HA microspheres, silica hollow microspheres are synthesized in water/hexane/water emulsions with Span 80 and Tween 80 [29]. The authors think that the hollow microsphere of hydroxyapatite in the present study was also synthesized in W/O/W

https://doi.org/10.1016/j.heliyon.2019.e01490

emulsion although the microdroplets (probably around 1 μm in size) of the inner water in oil phase could not be observed by optical microscopy.

The crystalline phase of the nanoparticles was identified by XRD (Fig. 2). The diffraction lines of the synthesized hollow microspheres approximately coincided with the HA standard [30, 31] and commercially available HA microrods, although the peaks were broad and some of them overlapped to form broader peaks. The peak broadening is attributed to the size of the HA nanocrystals in the hollow microsphere [17]. The full width at half maximum of peaks are known to be inversely proportional to crystalline sizes as shown by the Scherrer formula [32] although we did not calculate the crystalline sizes because of the overlapping of the peaks. Fig. 3 shows the IR spectra. The bands at 561, 602, 961, 1032, and 1090 cm^{-1} were assigned to PO_4^{3-}. A small shoulder of OH^- existed at approximately 630 cm^{-1} [30,33]. The IR spectrum of the hollow microsphere coincided with that of the commercially available HA microrods and that of the HA hollow microspheres reported by a previous study [17]. Note that the bands at 874, 1416, at 1547 cm^{-1} suggests that the HA microrods were carbonate-incorporated apatite [34]. The deposition of carbonate ions may have occurred in the manufacturing because the IR spectrum of HA microrods was measured with the samples from a freshly opened bottle. The data presented in Figs. 1, 2, and 3 demonstrate that the HA hollow microspheres can be prepared with $CaCl_2$ and K_2HPO_4 using the W/O/W emulsion method.

Fig. 4 shows the SEM images of the HA hollow microspheres and microrods. The size and specific area of the HA hollow microspheres and microrods are summarized in Table 1. Both particles had a size of approximately one micrometer and could thus be easily recovered by centrifugation at a low centrifugal acceleration (typically

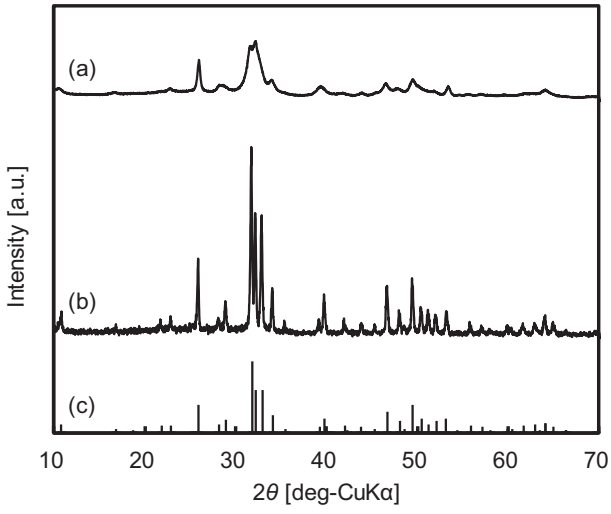

Fig. 2. XRD patterns of the synthesized HA hollow microspheres (a), commercially available HA microrods (b), and HA standard data (ICDD 9−432) (c).

https://doi.org/10.1016/j.heliyon.2019.e01490

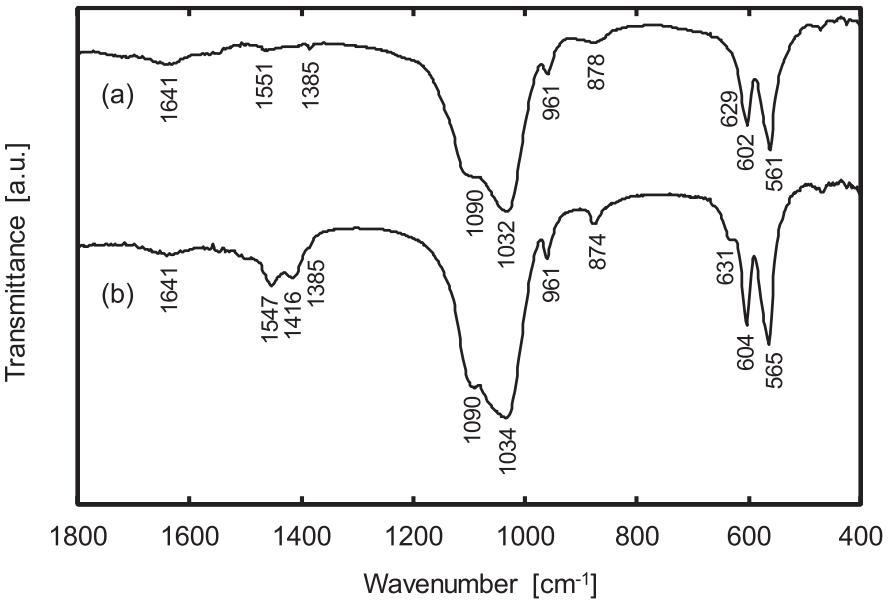

Fig. 3. FTIR spectra of HA hollow microspheres (a) and HA microrods (b).

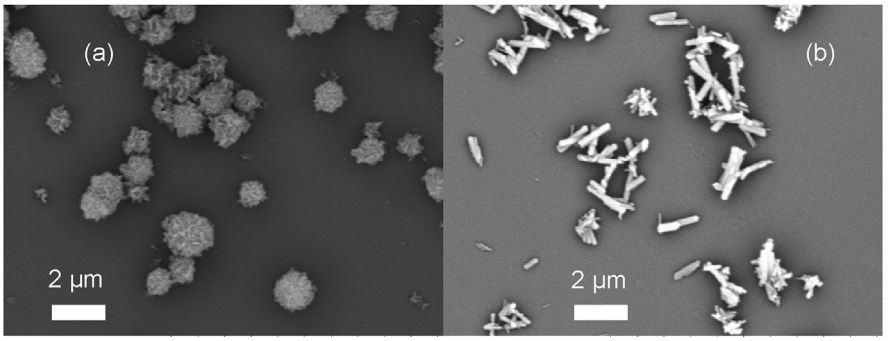

Fig. 4. SEM images of HA hollow microspheres (a) and HA microrods (b).

Table 1. Size and specific surface area of HA hollow microspheres and microrods.

Samples	HA hollow microspheres	HA microrods
		Long axis: 1.28 ± 0.36
Diameter [μm]	1.34 ± 0.29	Short axis: 0.31 ± 0.06
	(n = 1000)	(n = 100)
BET surface area [m^2/g]	150.30 ± 0.22	7.13 ± 0.03
Calculated surface area from diameter and axes [m^2/g]*	1.42**	4.58***

* Density of HA = 3.16 g/cm^3.

** Calculated as smooth solid spheres with a diameter of 1.34 μm.

*** Calculated as cylinders with a length of 1.28 μm and a diameter of 0.31 μm.

https://doi.org/10.1016/j.heliyon.2019.e01490

2000×g). Moreover, the specific surface area of the HA hollow microspheres measured experimentally by the N_2 adsorption was two orders higher than that calculated from the average diameter and density of the HA (3.16 g/cm^3) [31,35] with the assumption of solid (not hollow) particles. The high specific area of the HA hollow microspheres is attributed to the nanoparticle-assembled structure. Note that the measured specific area of the HA microrods was comparable with the calculated value.

3.2. Adsorption and desorption of bovine serum albumin and bovine γ-globulin on HA hollow microspheres

HA is used for the adsorption of various biomacromolecules including proteins and nucleic acids. Proteins are typically adsorbed in 1−10 mM sodium (or potassium) phosphate buffer at pH 6−7 and recovered by a 200−500 mM phosphate buffer at the same pH. Some of the additives in the buffer, e.g., NaCl, $CaCl_2$, and poly (ethylene glycol), improve the elution of the adsorbed proteins [2, 36, 37, 38, 39, 40]. In this study 10 mM and 800 mM sodium phosphate buffers at pH 6.8 were used in the adsorption and desorption (elution) of the proteins, respectively. Fig. 5 shows the dependence of the adsorption and desorption of bovine serum albumin and bovine γ-globulin on the hollow microspheres and microrods of HA. The 20 mg of the hollow microspheres almost completely adsorbed the protein in 1 mL of 10 mM sodium phosphate buffer (pH 6.8) when the concentration was 1 mg/mL or lower. The amounts of bovine serum albumin adsorbed on the HA microrods were one third or less of those adsorbed on the HA hollow microspheres. The adsorption of bovine γ-globulin on both adsorbents was higher than that of bovine serum albumin at high initial protein concentrations. The adsorbed proteins were desorbed from both HA particles by 800 mM sodium phosphate buffer (pH 6.8). In the experiments shown in Fig. 5(a), the amounts of adsorbed proteins were not sufficiently accurate when the adsorption ratio was low. The low accuracy is attributed to the calculation, wherein the adsorbed amounts are calculated by subtracting the residual amount of proteins from the initial amount in the solution. Thus, some amounts of desorbed proteins were higher than the amounts of adsorbed proteins, particularly in the adsorption and desorption of bovine serum albumin on the microrods. Regardless of the above experimental limitation, the 800 mM phosphate buffer was found to be an effective eluent for desorbing the proteins adsorbed on both the HA hollow microspheres and the HA microrods.

3.3. Adsorption isotherms of HA hollow microspheres for different proteins

Fig. 6 shows the adsorption isotherms of the HA hollow microspheres for bovine serum albumin, bovine γ-globulin, equine skeletal muscle myoglobin, and chicken

https://doi.org/10.1016/j.heliyon.2019.e01490

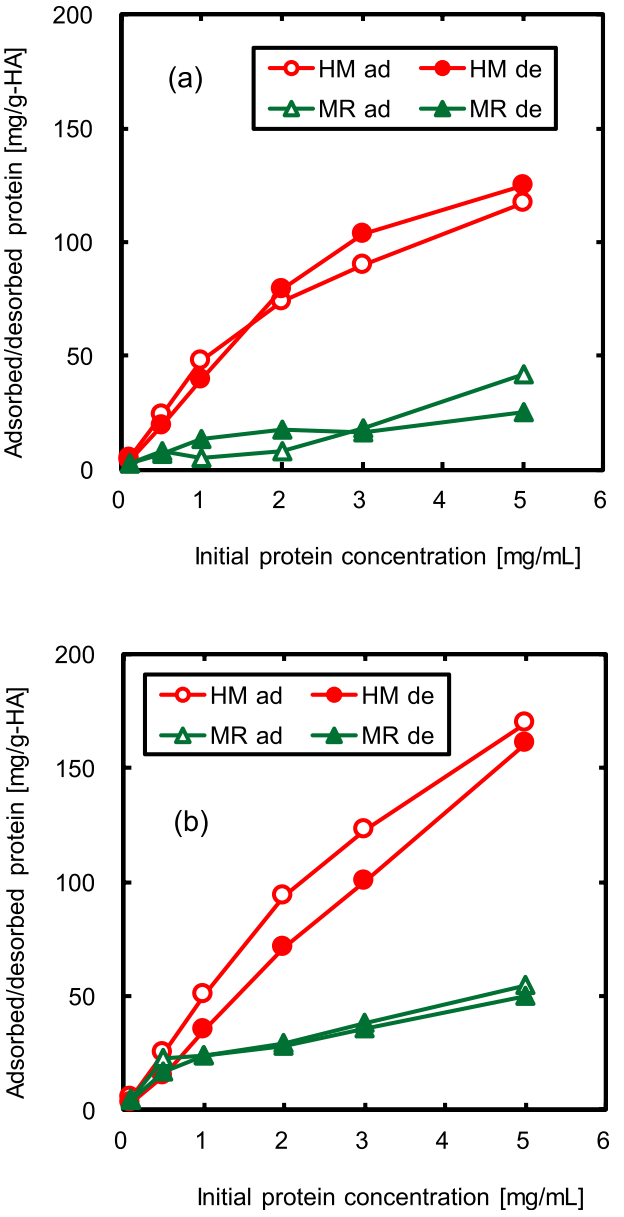

Fig. 5. Dependence of protein adsorption (ad) and desorption (de) on HA hollow microspheres (HM) and microrods (MR) on initial protein concentration: (a) bovine serum albumin and (b) bovine γ-globulin. In this experiment, the mass of HAs and the volume of the protein solutions were 20 mg and 1 mL, respectively.

egg white lysozyme in 10 mM sodium phosphate buffer (pH 6.8). The isotherms of the HA microrods are also shown for comparison. The concentration and volume of the protein solutions were changed in the experiments so that the protein adsorption ratios were 5−95%. The reason of the change in volume is that the residual protein concentrations after adsorption were too low to determine at the initial concentrations lower than 1 mg/mL when the solution volume was 1 mL (Fig. 5). The charges of the four proteins were different at pH 6.8 because of their different isoelectric

https://doi.org/10.1016/j.heliyon.2019.e01490

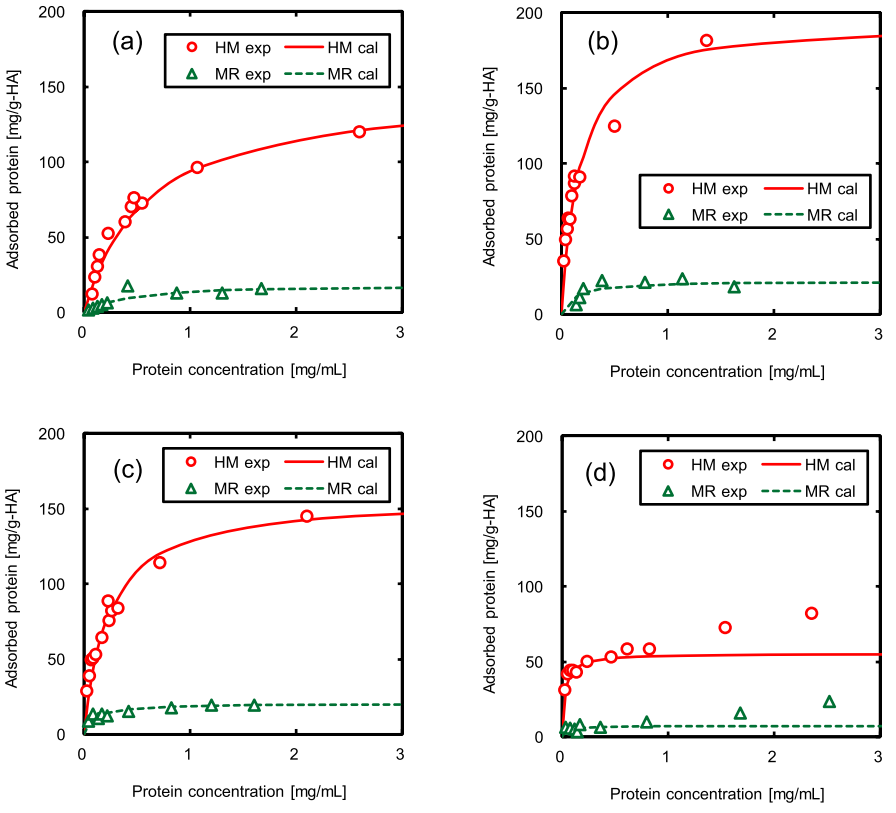

Fig. 6. Protein adsorption on HA hollow microspheres (HM) and microrods (MR). Protein concentrations are those after adsorption. Lines (HM cal and MR cal) show Langmuir type adsorption isotherms fitted to each experimental data (HM exp and MR exp): (a) bovine serum albumin, (b) bovine γ-globulin, (c) equine skeletal muscle myoglobin, and (d) chicken egg white lysozyme. Note that the lines in Fig. 6(d) are calculated from the experimental data at $C < 0.5$ mg/mL.

points (Table 2). However, the negative (bovine serum albumin), nearly neutral (bovine γ-globulin and equine skeletal muscle myoglobin), and positive (chicken egg white lysozyme) were adsorbed on both the hollow microspheres and the microrods (Fig. 6). This is attributed to the fact that the surfaces of the HA crystals have positive (Ca^{2+}) and negative (PO_4^{3-}, OH^-) sites, although the ratio of the sites depends on the crystalline face [55]. The adsorption of proteins with different charges on the HA surfaces at neutral pH is shown in Fig. 7.

The adsorption behaviors of the four proteins on both of the hollow microspheres and microrods of HA approximately exhibited Langmuir type isotherms, where the molecules were adsorbed on the adsorbent in a monolayer at a maximum, as follows:

$$q = \frac{q_m k C}{1 + kC} \tag{1}$$

https://doi.org/10.1016/j.heliyon.2019.e01490

Table 2. Protein properties and Langmuir parameters for adsorption of proteins on HA hollow microspheres and microrods.

Proteins	HA hollow microspheres	HA microrods
Bovine serum albumin		
(m.w. = 66.4 kDa,[a])	q_m = 148 mg/g-HA	q_m = 19 mg/g-HA
14.1 × 4.2 × 4.2 nm,[b])	K = 1.7 mL/mg	k = 2.5 mL/mg
pI = 4.7–4.9,[c])	(r = 0.98)	(r = 0.96)
$n_{m,theor}$ = 2.5 mg/m^2.[d])	n_m = 0.98 mg/m^2	n_m = 2.7 mg/m^2
Bovine γ-globulin		
(m.w. = 163 &150 kDa*,[e])	q_m = 199 mg/g-HA	q_m = 22 mg/g-HA
23.5 × 4.4 × 4.4 nm†,[f])	k = 5.5 mL/mg	k = 8.6 mL/mg
pI = 5.5–6.8 & 7.5–8.3*,[g])	(r = 0.99)	(r = 0.96)
$n_{m,theor}$ = 2.0–5.5 mg/m^2.[h])	n_m = 1.32 mg/m^2	n_m = 3.1 mg/m^2
Equine skeletal muscle myoglobin		
(m.w. = 17.6 kDa,[i])	q_m = 158 mg/g-HA	q_m = 21 mg/g-HA
4.5 × 3.5 × 2.5 nm‡,[j])	k = 4.4 mL/mg	k = 9.6 mL/mg
pI = 7.3,[k])	(r = 1.00)	(r = 1.00)
$n_{m,theor}$ = 2.4 mg/m^2.[l])	n_m = 1.05 mg/m^2	n_m = 3.0 mg/m^2
Chicken egg white lysozyme		
(m.w. = 14.3 kDa,[m])	q_m = 56 mg/g-HA¶	q_m = 7.0 mg/g-HA¶
4.5 × 3.0 × 3.0 nm,[j])	k = 35.0 mL/mg¶	k = 33.4 mL/mg¶
pI = 11.35,[n])	(r = 1.00) ¶	(r = 0.91) ¶
$n_{m,theor}$ = 2.0 mg/m^2.[d])	n_m = 0.37 mg/m^2¶	n_m = 1.0 mg/m^2¶

q_m: maximum adsorption capacity; k: equilibrium constant.
r: correlation coefficient for the C/q-C plots.
n_m: maximum adsorption capacity per BET surface area.
$n_{m,theor}$: theoretical values of n_m in the literature.
* Values of bovine IgG1 and IgG2, respectively.
† Values of human γ-globulin.
‡ Values of sperm whale myoglobin.
¶ The values were calculated from experimental data at $C < 0.5$ mg/mL.

Data source: a) Hirayama et al., 1990 [41]; b) Wright and Thompson, 1975 [42]; c) Malamud and Drysdale, 1978 [43]; d) Kandori et al., 2002 [44]; e) Butler, 1969 [45]; f) Oncley et al., 1947 [46]; g) Josephson et al., 1972 [47]; h) Buijs et al., 1995 [48]; i) Katta and Chait, 1991 [49]; j) Bodo et al., 1959 [50]; k) Radola, 1973 [51]; l) Kandori, 2000 [52]; m) Canfield, 1963 [53]; n) Wetter et al., 1951 [54].

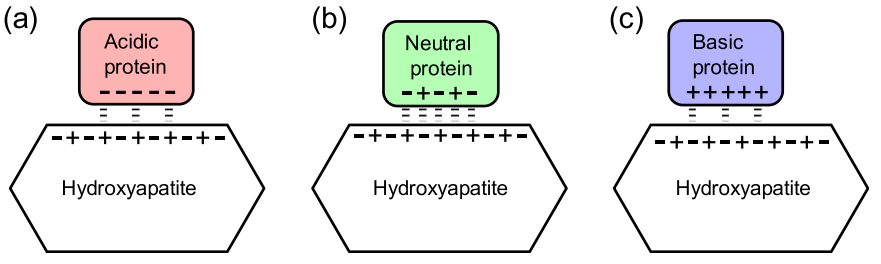

Fig. 7. Adsorption of acidic (pI < 5) (a), neutral (pI ≈ 7) (b), and basic (pI > 9) (c) proteins on hydroxyapatite at neutral pH.

https://doi.org/10.1016/j.heliyon.2019.e01490

where q is the adsorbate mass per adsorbent mass, C is the equilibrium concentration of the adsorbate, q_m is the maximum adsorption capacity, and k is the affinity parameter. The C/q-C plot(s) and the method of least squares were used to calculate q_m and k with Eq. (2).

$$\frac{C}{q} = \frac{1}{q_m}C + \frac{1}{q_m k} \tag{2}$$

The calculated values of q_m and k are summarized in Table 2, where the molecular weights (m.w.) and isoelectric points (pI) previously reported in the literature are also shown. The q calculated using Eq. (1) with q_m, k, and C, is represented by the solid and broken curves shown in Fig. 6. The calculated curves fit well with the experimental values. The maximum adsorption capacities q_m of the HA hollow microspheres were 7.5−9.0 times higher than those of the HA microrods for the corresponding proteins. Conversely, the adsorption capacities per the BET surface area (n_m) of the HA hollow microspheres were lower than those of the HA microrods. This is attributed to the nanoparticle-assembled structure of the HA hollow microspheres; there existed surfaces where small nitrogen molecules were adsorbed but much larger protein molecules were not on the surface of the nanoparticles, as shown in Fig. 8. This observation is in agreement with the results presented by Kandori

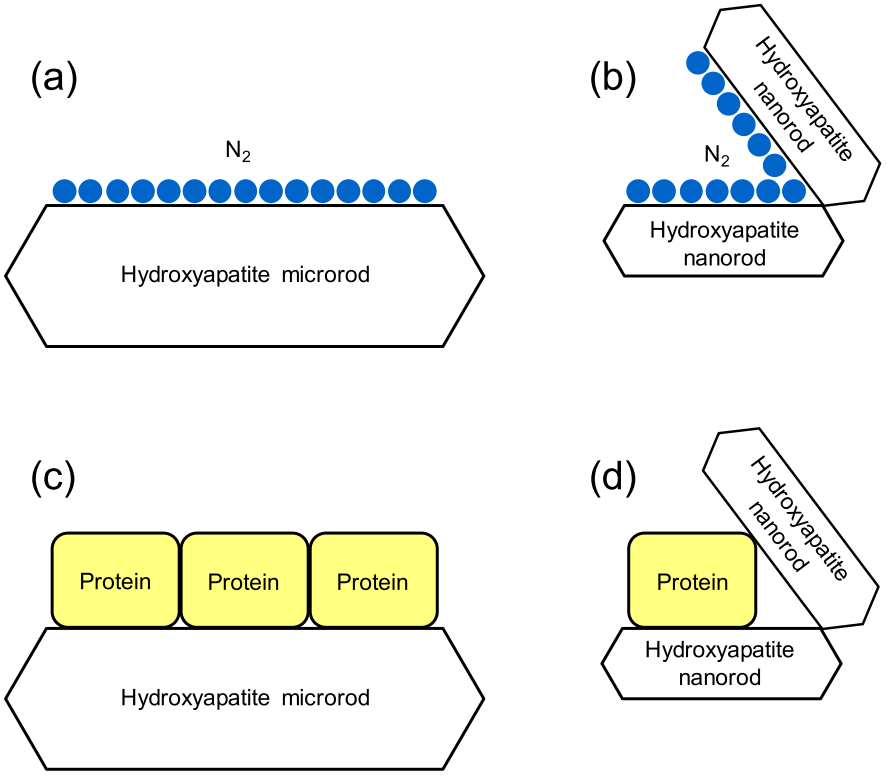

Fig. 8. Adsorption of N_2 (a, b; in measurement of BET surface area) and proteins (c, d) on HA microrod (a, c) and nanorod-assembled microparticle (b, d).

https://doi.org/10.1016/j.heliyon.2019.e01490

et al. [56], who reported that the value of n_m decreases as the surface area of a single HA particle decreases. Note that the maximum adsorption capacities of the HA microrods are comparable with the theoretical values ($n_{m,theor}$) previously reported in the literature (Table 2), because the microrods have plain surface areas that are much larger than those of the proteins adsorbed on the crystal surface (Fig. 4(b) and Table 1). On the other hand, the equilibrium constants k of the HA hollow microspheres for the four proteins are comparable with those of the HA microrods for the corresponding proteins. The values of k express the affinities of the HA surfaces with the proteins. Note that the affinities of the *ac* and *ab* crystal faces (*a*- and *c*-planes) of the HA toward proteins are different [56, 57, 58]. The Ca-rich and positively charged *ac* crystal face (*a*-plane) preferentially adsorbs negative proteins, while the P-rich and negatively charged *ab* crystal face (*c*-plane) preferentially adsorbs positive proteins. Additionally, the protein charges were different owing to the number and location of the charged amino acid residues in the proteins, and the pH in the adsorption experiments. Thus, the analysis regarding the dependence of the k values on the HA crystals and proteins is difficult. However, the comparable k values of the HA hollow microspheres and HA microrods for each protein at pH 6.8 in 10 mM sodium phosphate buffer suggest that the area ratios of the *ac* and *ab* crystal surfaces (*a*- and *c*-planes) are comparable for the two adsorbents. This would be attributed to the similar shape between the nanoparticles in the HA hollow microspheres (Fig. 1) and the microparticles of commercially available HA (Fig. 4(b)), although both rod-shaped particles had different size.

3.4. Protein adsorption/desorption by HA-PLLA composite membranes

The hollow HA microspheres were integrated into a microporous membrane for the adsorbent in membrane chromatography. In the integration carried out in this study, a PLLA porous membrane with open finger-like pores was used as the membrane. The membrane structure becomes suitable for the facile composition of the microspheres and porous membrane by filtering a suspension of the microspheres [28, 59]. Fig. 9 shows the cross-section of the composite membrane. The open finger-like pores had the HA microspheres (Figs. 9(a) and (f)). Elemental analysis by EDS also found the Ca and P atoms of the HA in the pores (Figs. 9(e, g), and (h)). HA microspheres were not observed in the closed pores (Figs. 9(b, c, d)). The integrated volume was estimated as approximately half of the membrane (Fig. 9(a)). We used this composite membrane for membrane chromatography, although the volume would be enhanced by the improvement of the membrane structure.

Fig. 10 shows the adsorption and desorption of the bovine serum albumin and bovine γ-globulin on the HA-PLLA composite membranes. The bovine γ-globulin (50 μg/mL) in 10 mL of 10 mM sodium phosphate buffer (pH 6.8) was

https://doi.org/10.1016/j.heliyon.2019.e01490

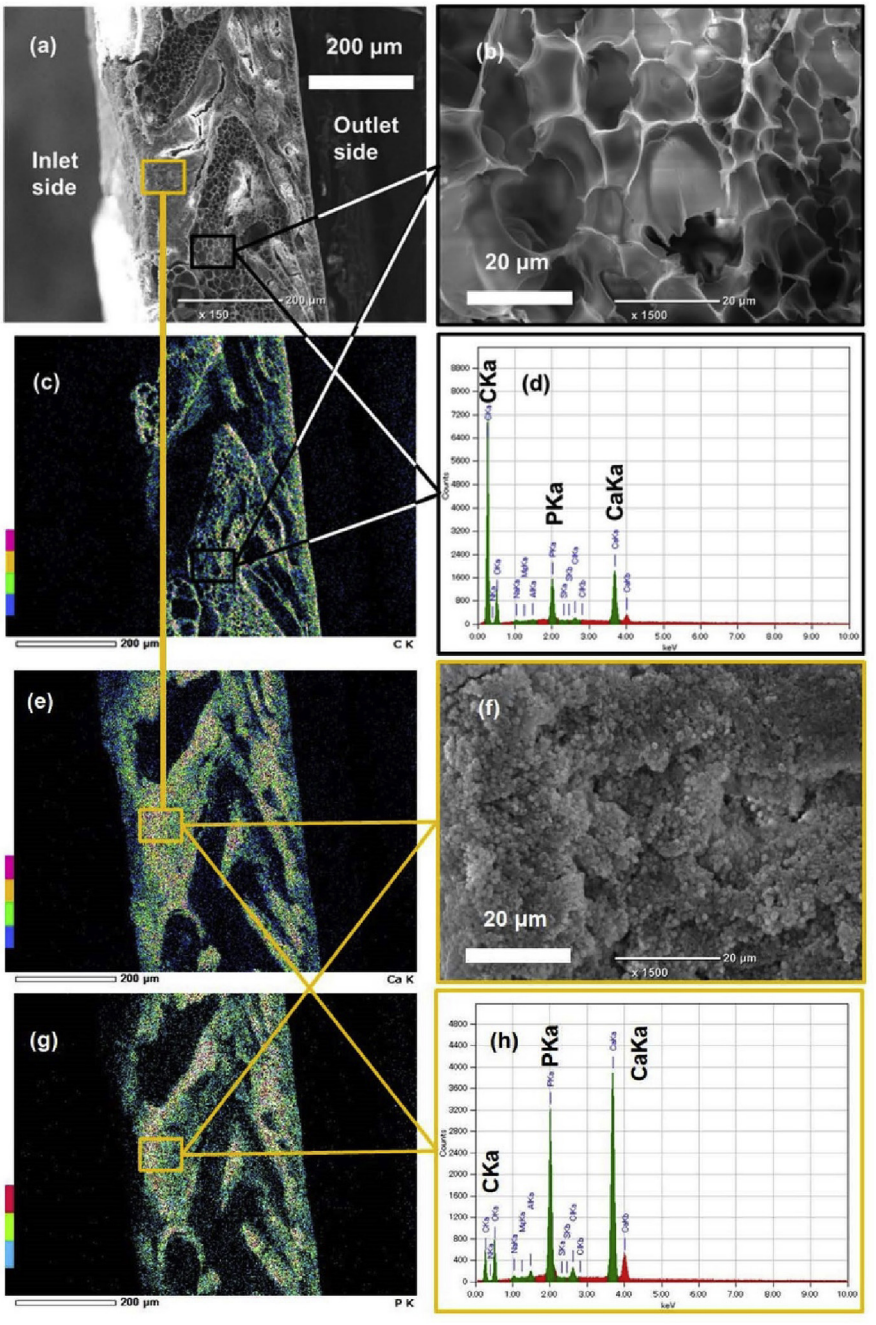

Fig. 9. SEM images and EDS analysis of HA microspheres in a PLLA membrane. (a) Cross-section of PLLA membrane containing HA hollow microspheres, (b) magnified view of a PLLA part, (c) carbon-mapping, (d) elemental analysis of PLLA part, (e) calcium-mapping, (f) magnified view of a HA part, (g) phosphorus-mapping, (h) elemental analysis of HA part.

adsorbed on the membrane completely, whereas only 17% of the bovine serum albumin was adsorbed on the membrane under the same conditions. The difference is attributed to the higher affinity parameter (equilibrium constant) k of HA for the bovine γ-globulin although the maximum adsorption capacities q_m of both

https://doi.org/10.1016/j.heliyon.2019.e01490

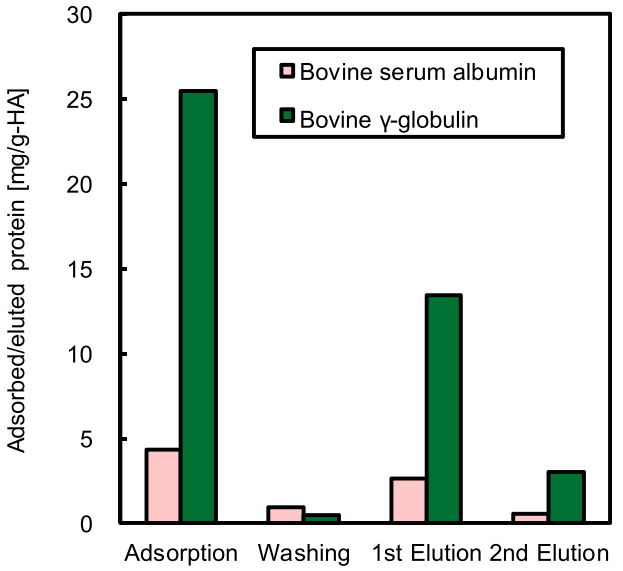

Fig. 10. Protein adsorption and elution on HA-PLLA composite membranes.

proteins are comparable (Table 2). After washing with 1 mL of 10 mM sodium phosphate buffer, the adsorbed proteins were recovered with 2 mL (1 mL × 2) of 800 mM sodium phosphate buffer. The adsorbed γ-globulin was recovered by 66%, whereas the adsorbed bovine serum albumin was recovered by 96%. The γ-globulin with a high equilibrium constant to the HA hollow microsphere was concentrated 3.3 times (= (10 mL/2 mL)×(66/100)) by the HA-PLLA composite membrane. However, in future work, the recovery should be enhanced by improving the preparation of the composite membranes and the adsorption and elution conditions [37, 38].

4. Conclusions

The nanoparticle-assembled HA hollow microspheres synthesized from $CaCl_2$ and K_2HPO_4 by a W/O/W emulsion method had 7.5−9.0 times higher adsorption capacities for proteins than did the HA microrods of similar size. This is attributed to the higher BET specific area of the hollow microspheres, rather than that of the microrods, although the maximum adsorption capacities per the BET surface area of the former were lower than those of the latter. For each protein, the affinity parameters of the HA hollow microspheres were comparable to those of the HA microrods. The HA hollow microspheres integrated a microporous membrane with open finger-like pores by filtration. The composite membranes of the HA hollow microspheres and the PLLA microporous membrane showed a high adsorption capacity for γ-globulin and the concentrated protein was recovered with an elution buffer.

https://doi.org/10.1016/j.heliyon.2019.e01490

Declarations

Author contribution statement

Takaaki Tanaka: Conceived and designed the experiments; Performed the experiments; Analyzed and interpreted the data; Contributed reagents, materials, analysis tools or data; Wrote the paper.

Yoshihiko Takai, Akifumi Nagase, Kazuki Teraguchi, Hiromi Minbu: Performed the experiments; Analyzed and interpreted the data.

Akihitio Ochiai: Analyzed and interpreted the data.

Isao Kimura: Conceived and designed the experiments; Analyzed and interpreted the data; Contributed reagents, materials, analysis tools or data; Wrote the paper.

Masayuki Taniguchi: Analyzed and interpreted the data; Wrote the paper.

Funding statement

Takaaki Tanaka was supported by Grants-in-Aid for Scientific Research from the Japan Society for the Promotion of Science (JSPS KAKENHI, Grant Numbers: JP17K06921, JP21560807, and JP24560957).

Competing interest statement

The authors declare no conflict of interest.

Additional information

No additional information is available for this paper.

Acknowledgements

The authors thank Toyota Motor Corp. for kindly gifting the PLLA polymer. The TEM images were taken by courtesy of Prof. Hiromi Konishi of Niigata University.

References

[1] J.R. Porter, T.T. Ruckh, K.C. Popat, Bone tissue engineering: a review in bone biomimetics and drug delivery strategies, Biotechnol. Prog. 25 (2009) 1539−1560.

[2] M.J. Gorbunoff, Protein chromatography on hydroxyapatite columns, Methods Enzymol. 117 (1985) 370−380.

https://doi.org/10.1016/j.heliyon.2019.e01490

[3] A. Szcześ, L. Hołysz, E. Chibowski, Synthesis of hydroxyapatite for biomedical applications, Adv. Colloid Interface Sci. 249 (2017) 321–330.

[4] A. Haider, S. Haider, S.S. Han, I. Kang, Recent advances in the synthesis, functionalization and biomedical applications of hydroxyapatite: a review, RSC Adv. 7 (2017) 7442–7458.

[5] K. Lin, C. Wu, J. Chang, Advances in synthesis of calcium phosphate crystals with controlled size and shape, Acta Biomater. 10 (2014) 4071–4102.

[6] W. Lai, C. Chen, X. Ren, I. Lee, G. Jiang, X. Kong, Hydrothermal fabrication of porous hollow hydroxyapatite microspheres for a drug delivery system, Mater. Sci. Eng. C 62 (2016) 166–172.

[7] M. Sadat-Shojai, M.T. Khorasani, E. Dinpanah-Khoshdargi, A. Jamshidi, Synthesis methods for nanosized hydroxyapatite with diverse structures, Acta Biomater. 9 (2013) 7591–7621.

[8] S. Mondal, S.V. Dorozhkin, U. Pal, Recent progress on fabrication and drug delivery applications of nanostructured hydroxyapatite, WIREs Nanomed. Nanobiotechnol. 10 (2018) e1504.

[9] R. Sun, Y. Lu, K. Chen, Preparation and characterization of hollow hydroxyapatite microspheres by spray drying method, Mater. Sci. Eng. C 29 (2009) 1088–1092.

[10] M.G. Ma, J.F. Zhu, Solvothermal synthesis and characterization of hierarchically nanostructured hydroxyapatite hollow spheres, Eur. J. Inorg. Chem. 2009 (2009) 5522–5526.

[11] C. Qi, Y.J. Zhu, B.Q. Lu, X.Y. Zhao, J. Zhao, F. Chen, J. Wu, Hydroxyapatite hierarchically nanostructured porous hollow microspheres: rapid, sustainable microwave-hydrothermal synthesis by using creatine phosphate as an organic phosphorus source and application in drug delivery and protein adsorption, Chem. Eur. J. 19 (2013) 5332–5341.

[12] M.Y. Ma, Y.J. Zhu, L. Li, S. Cao, Nanostructured porous hollow ellipsoidal capsules of hydroxyapatite and calcium silicate: preparation and application in drug delivery, J. Mater. Chem. 18 (2008) 2722–2727.

[13] W. Qiao, X. Lan, J.K.H. Tsoi, Z. Chen, R.Y.X. Su, K.W.K. Yeung, J.P. Matinlinn, Biomimetic hollow mesoporous hydroxyapatite microsphere with controlled morphology, entrapment efficiency and degradability for cancer therapy, RSC Adv. 7 (2017) 44788–44798.

https://doi.org/10.1016/j.heliyon.2019.e01490

[14] S. Safi, F. Karimzadeh, S. Labbaf, Mesoporous and hollow hydroxyapatite nanostructured particles as a drug delivery vehicle for the local release of ibuprofen, Mater. Sci. Eng. C 92 (2018) 712–719.

[15] H. Fu, M.N. Rahaman, D.E. Day, Effect of process variables on the microstructure of hollow hydroxyapatite microspheres prepared by a glass conversion method, J. Am. Ceram. Soc. 93 (2010) 3116–3123.

[16] Y. Wang, A. Yao, W. Huang, D. Wang, J. Zhou, In situ fabrication of hollow hydroxyapatite microspheres by phosphate solution immersion, J. Cryst. Growth 327 (2011) 245–250.

[17] I. Kimura, T. Honma, R.E. Riman, Preparation of hydroxyapatite microspheres by interfacial reaction in a multiple emulsion, J. Ceram. Soc. Jpn. 115 (2007) 888–893.

[18] F. Ye, H. Guo, H. Zhang, X. He, Polymeric micelle-templated synthesis of hydroxyapatite hollow nanoparticles for a drug delivery system, Acta Biomater. 6 (2010) 2212–2218.

[19] D. Hagmeyer, K. Ganesan, J. Ruesing, D. Schunk, C. Mayer, A. Dey, et al., Self-assembly of calcium phosphate nanoparticles into hollow spheres induced by dissolved amino acids, J. Mater. Chem. 21 (2011) 9219–9223.

[20] T. Kawai, H. Sekikawa, H. Unuma, Preparation of hollow hydroxyapatite microspheres utilizing poly(divinylbenzene) as a template, J. Ceram. Soc. Jpn. 117 (2009) 340–343.

[21] B.P. Bastakoti, M. Inuoe, S. Yusa, S.H. Liao, K.C. Wu, K. Nakashima, Y. Yamauchi, A block copolymer micelle template for synthesis of hollow calcium phosphate nanospheres with excellent biocompatibility, Chem. Commun. 48 (2012) 6532–6534.

[22] C. Qi, Y.J. Zhu, B.Q. Lu, X.Y. Zhao, J. Zhao, F. Chen, Hydroxyapatite nanosheet-assembled porous hollow microspheres: DNA-templated hydrothermal synthesis, drug delivery and protein adsorption, J. Mater. Chem. 22 (2012) 22642–22650.

[23] M. Huang, Y. Wang, Synthesis of calcium phosphate microcapsules using yeast-based biotemplate, J. Mater. Chem. 22 (2012) 626–630.

[24] I. Kimura, T. Wei, Y. Kikushima, R.E. Riman, T. Akazawa, Effects of organic additives on the morphology of various calcium phosphates prepared via solution and emulsion methods, IOP Conf. Ser. Mater. Sci. Eng. 18 (2011) 192017.

https://doi.org/10.1016/j.heliyon.2019.e01490

[25] W.C. Griffin, Calculation of HLB values of non-ionic surfactants, J. Soc. Cosmet. Chem. 5 (1954) 249–256. http://journal.scconline.org//pdf/cc1954/cc005n04/p00249-p00256.pdf.

[26] M. Capdevila, A. Maestro, M. Porras, J.M. Gutiérrez, Preparation of Span 80/oil/water highly concentrated emulsions: influence of composition and formation variables and scale-up, J. Colloid Interface Sci. 345 (2010) 27–33.

[27] V.V. Erramreddy, S. Ghosh, Influence of emulsifier concentration on nanoemulsion gelation, Langmuir 30 (2014) 11062–11074.

[28] H. Minbu, A. Ochiai, T. Kawase, M. Taniguchi, D.R. Lloyd, T. Tanaka, Preparation of poly(L-lactic acid) microfiltration membranes by a nonsolvent-induced phase separation method with the aid of surfactants, J. Membr. Sci. 479 (2015) 85–94.

[29] M. Fujiwara, K. Shiokawa, Y. Tanaka, Y. Nakahara, Preparation and formation mechanism of silica microcapsules (hollow sphere) by water/oil/water interfacial reaction, Chem. Mater. 16 (2004) 5420–5426.

[30] M. Markovic, B.O. Fowler, M.S. Tung, Preparation and comprehensive characterization of a calcium hydroxyapatite reference material, J. Res. Natl. Inst. Stand. Technol. 109 (2004) 553–568.

[31] International Center for Diffraction Data, ICDD File No. 9-432.

[32] A.L. Patterson, The Scherrer formula for X-ray particle size determination, Phys. Rev. 56 (1939) 978–982.

[33] C.B. Baddiel, E.E. Berry, Spectra structure correlations in hydroxy and fluorapatite, Spectrochim. Acta 22 (1966) 1407–1416.

[34] J. Wu, S. Hayakawa, K. Tsuru, A. Osaka, In vitro bioactivity of anatase film obtained by direct deposition from aqueous titanium tetrafluoride solutions, Thin Solid Films 414 (2002) 283–288.

[35] M. Yoshimura, H. Suda, Hydrothermal processing of hydroxyapatite: past, present, and future, in: P.W. Brown, B. Constantz (Eds.), Hydroxyapatite and Related Materials, CRC Press, Boca Raton, 1994, pp. 45–72.

[36] T. Kawasaki, S. Takahashi, K. Ikeda, Hydroxyapatite high-performance liquid chromatography: column performance for proteins, Eur. J. Biochem. 152 (1985) 361–371.

[37] A. Jungbauer, R. Hahn, K. Deinhofer, P. Luo, Performance and characterization of a nanophased porous hydroxyapatite for protein chromatography, Biotechnol. Bioeng. 87 (2004) 364–375.

https://doi.org/10.1016/j.heliyon.2019.e01490

[38] P. Gagnon, Monoclonal antibody purification with hydroxyapatite, N. Biotech. 25 (2009) 287–293.

[39] T. Nakagawa, T. Ishihara, H. Yoshida, T. Yoneya, K. Wakamatsu, T. Kadoya, Relationship between human IgG structure and retention time in hydroxyapatite chromatography with sodium chloride gradient elution, J. Sep. Sci. 33 (2010) 2045–2051.

[40] R. Freitag, F. Hlibrig, Isolation and purification of recombinant proteins, antibodies and plasmid DNA with hydroxyapatite chromatography, Biotechnol. J. 7 (2012) 90–102.

[41] K. Hirayama, S. Akashi, M. Furuya, K. Fukuhara, Rapid confirmation and revision of the primary structure of bovine serum albumin by ESIMS and frit-FAB LC/MS, Biochem. Biophys. Res. Commun. 173 (1990) 639–646.

[42] A.K. Wright, M.R. Thompson, Hydrodynamic structure of bovine serum albumin determined by transient electric birefringence, Biophys. J. 15 (1975) 137–141.

[43] D. Malamud, J.W. Drysdale, Isoelectric points of proteins: a table, Anal. Biochem. 86 (1978) 620–647.

[44] K. Kandori, A. Fudo, T. Ishikawa, Study on the particle texture dependence of protein adsorption by using synthetic micrometer-sized calcium hydroxyapatite particles, Colloids Surf., B 24 (2002) 145–153.

[45] J.E. Butler, Bovine immunoglobulins: a review, J. Dairy Sci. 52 (1969) 1895–1909.

[46] J.L. Oncley, G. Scatchard, A. Brown, Physical-chemical characteristics of certain of the proteins of normal human plasma, J. Phys. Chem. 51 (1947) 184–198.

[47] R.V. Josephson, E.M. Mikolajick, D.P. Sinha, Gel isoelectric focusing of selected bovine immunoglobulins, J. Dairy Sci. 55 (1972) 1508–1510.

[48] J. Buijs, J.W.T. Lichtenbelt, W. Norde, J. Lyklema, Adsorption of monoclonal IgGs and their F(ab')$_2$ fragments onto polymeric surfaces, Colloids Surf. B 5 (1995) 11–23.

[49] V. Katta, B.T. Chait, Observation of the heme-globin complex in native myoglobin by electrospray-ionization mass spectrometry, J. Am. Chem. Soc. 113 (1991) 8534–8535.

https://doi.org/10.1016/j.heliyon.2019.e01490

[50] G. Bodo, H.M. Dintzis, J.C. Kendrew, H.W. Wyckoff, The crystal structure of myoglobin, V. A low-resolution three-dimensional Fourier synthesis of sperm-whale myoglobin crystals, Proc. Roy. Soc. Lond. A 253 (1959) 70−102.

[51] B.J. Radola, Isoelectric focusing in layers of granulated gels. I. Thin-layer isoelectric focusing of proteins, Biochim. Biophys. Acta 295 (1973) 412−428.

[52] K. Kandori, A. Fudo, T. Ishikawa, Adsorption of myoglobin onto various synthetic hydroxyapatite particles, Phys. Chem. Chem. Phys. 2 (2000) 2015−2020.

[53] R.E. Canfield, The amino acid sequence of egg white lysozyme, J. Biol. Chem. 238 (1963) 2698−2707. http://www.jbc.org/content/238/8/2698.full.pdf.

[54] L.R. Wetter, H.F. Deutsch, Immunological studies on egg white proteins. IV. Immunochemical and physical studies of lysozyme, J. Biol. Chem. 192 (1951) 237−242. http://www.jbc.org/content/192/1/237.full.pdf.

[55] K. Kandori, K. Miyanaga, T. Ishikawa, Adsorption of immunogamma globulin onto various synthetic calcium hydroxyapatite particles, J. Colloid Interface Sci. 273 (2004) 406−413.

[56] K. Kandori, H. Hamazaki, M. Matsuzawa, S. Togashi, Selective adsorption of acidic protein of bovine serum albumin onto sheet-like calcium hydroxyapatite particles produced by microreactor, Adv. Powder Technol. 25 (2014) 354−359.

[57] Z. Zhuang, M. Aizawa, Protein adsorption on single-crystal hydroxyapatite particles with preferred orientation to *a(b)*- and *c*-axes, J. Mater. Sci. Mater. Med. 24 (2013) 1211−1216.

[58] M. Aizawa, T. Matsuura, Z. Zhuang, Syntheses of single-crystal apatite particles with preferred orientation to the *a*- and *c*-axes as models of hard tissue and their applications, Biol. Pharm. Bull. (2013) 1654−1661.

[59] H. Minbu, H. Mizuno, Y. Shibuya, A. Ochiai, M. Taniguchi, T. Tanaka, Poly(L-lactic acid) depth filter membrane prepared by nonsolvent-induced phase separation with the aid of a nonionic surfactant, J. Chem. Eng. Jpn. 52 (2019) 75−82.

https://doi.org/10.1016/j.heliyon.2019.e01490